

Exact distributions for bit error rate and channel capacity in free-space optical communication

Santosh Kumar¹ ✉, Rajeev Kumar Singh¹, Karmeshu¹

¹Shiv Nadar University, Gautam Buddha Nagar, UP 201314, India

✉ E-mail: skumar.physics@gmail.com

ISSN 1751-8628

Received on 20th March 2019

Revised 17th June 2019

Accepted on 20th August 2019

E-First on 24th September 2019

doi: 10.1049/iet-com.2019.0314

www.ietdl.org

Abstract: Bit error rate (BER) and channel capacity are two important metrics to assess the performance of free-space optical communication (FSOC) systems. Due to the fading of the optical signal owing to the atmospheric effects, these two quantities behave as random variables. Most of the studies in this direction have focused on the calculation of only the average of these quantities. However, since the complete information about a random variable is encoded in its distribution, it is more informative to examine the latter itself. In this work, the authors derive exact probability density function (PDF) expressions for the BER and the channel capacity for an arbitrary irradiance model. In particular, they investigate these exact results for log-normal, gamma-gamma, and K distributions. For the BER analysis, they focus on the binary phase shift keying and quadrature phase shift keying modulation schemes. The authors' analytical results are found to be in conformity with Monte Carlo simulations. The exact PDFs of the BER and the channel capacity reveal that there are several instances when the average is unable to capture the actual behaviour of these quantities, and therefore one must be careful in drawing conclusions based on the first moment only.

1 Introduction

Free-space optical communication (FSOC) has generated considerable interest in recent times due to tremendous advantages it offers over radio-frequency communications [1–3]. This includes enhanced bandwidth, low power consumption, inexpensive and compact equipment, and greater security against eavesdropping. However, the atmospheric turbulence results in the fading of the optical signal, thereby degrading the performance of the communication systems.

There are several statistical models describing the atmospheric turbulence which quantify the irradiance of FSOC channels in a given turbulence scenario. A few prominent examples are the log-normal distribution [4–6], the K distribution [4, 5, 7–9], and the gamma-gamma distribution [4, 10–12]. The log-normal model applies to the case of relatively weak turbulence, whereas the K distribution has been found to describe the strong turbulence regime. Gamma-gamma distribution can be used in a wide range of turbulence conditions, ranging from weak to strong.

Once the behaviour of the irradiance is described by one of the appropriate fading models, the next logical step is to evaluate certain quality of service (QoS) measures to assess the performance of the communication system. Bit error rate (BER) and channel capacity are two such very important metrics [4, 13–15]. As a consequence of the stochastic nature of the optical signal, these quantities behave as random variables. Typically, investigation involving these measures remains restricted only to their respective averages (first moments) [4, 13–27]. However, since the full information concerning a random variable is encoded in its distribution, the average values may not capture the true behaviour of these metrics. The study of higher-order statistics of the above metrics beyond the first moment has been scarce, especially in the context of FSOC [28, 29].

In this work, we derive exact probability density function (PDF) expressions for the BER and the channel capacity. Our expressions are applicable to any fading model for the irradiance. However, for our analysis, we focus mainly on the log-normal, gamma-gamma, and K distributions. Interestingly, unlike the exact expressions for the averages, which contain higher transcendental functions like Meijer G [15, 16, 19, 25], our exact expressions for the PDFs involve relatively simple special functions. By evaluating these results we find that there are several instances when the PDF is not

'localised' around the average value and, instead, is rather dispersed. Consequently, the average is unable to capture the *actual* behaviour of the BER and channel capacity random variables, and necessitates computation of higher-order moments and PDF.

The presentation scheme in this paper is as follows. In Section 2, we outline the conventional channel model used for FSOC. Section 3 summarises three of the very popular PDFs for modelling the signal fading, namely, the log-normal distribution, the gamma-gamma distribution, and the K distribution. In Section 4, we present our exact result for the BER PDF. The exact result for the channel capacity PDF is presented in Section 5. While our exact results hold for an arbitrary irradiance model, we focus on the log-normal, gamma-gamma, and K distributions for our analysis in Sections 4 and 5. Moreover, for the BER analysis we consider the binary phase shift keying (BPSK) and quadrature phase shift keying (QPSK) modulation schemes. Finally, we conclude in Section 6 with a brief summary of our work.

2 Channel model

The communication channel for the optical signal is assumed to be memoryless, stationary, and ergodic, with independent and identically distributed intensity fast fading statistics. Within this statistical model, the received signal y is given by [13, 15]

$$y = \eta I x + n, \quad (1)$$

where η is the effective photo-current conversion ratio of the receiver, I is the normalised irradiance, x is the transmitted signal, and n is the white Gaussian noise with zero mean and variance $N_0/2$. The instantaneous electrical signal-to-noise ratio (SNR) can be defined as [6, 14],

$$\gamma = \frac{(\eta I)^2}{N_0}. \quad (2)$$

The average SNR is defined as $\bar{\gamma} = (\eta \mathbb{E}[I])^2 / N_0$, where $\mathbb{E}[\cdot]$ represents the expected or average value [6, 14]. It should be noted that, as per this conventional definition, $\bar{\gamma} \neq \mathbb{E}[\gamma] = (\eta^2 \mathbb{E}[I^2]) / N_0$. The signal reaching the receiver is faded on account of encountering turbulence. Consequently, I is modelled using one of

Table 1 Parameters for various modulation schemes

Modulation scheme	a	b
NRZ-OOK	2	$2\sqrt{2}$
RZ-OOK	2	2
L -PPM	2	$4/\sqrt{L\log_2 L}$
PAM	2	$2\sqrt{2}(L-1)/\sqrt{\log_2 L}$
BPSK	2	1
QPSK	1	1

the appropriate fading models [4, 6] as briefly discussed in Section 1.

3 Distribution models for the irradiance

In the following, we consider the log-normal, gamma-gamma, and the K distribution models for the irradiance, which are very popular distributions for describing the effects due to atmospheric turbulence in FSOC.

3.1 Log-normal distribution

In the case of a relatively weak turbulence, the light intensity fading may be modelled as a log-normal random variable [4, 6]. The corresponding PDF is given by [4, 11, 19]

$$f(I) = \frac{1}{\sqrt{2\pi}\sigma I} \exp\left(-\frac{(\ln I + \sigma^2/2)^2}{2\sigma^2}\right) \mathbb{1}_{(0,\infty)}, \quad (3)$$

where ‘ln’ represents the natural log (base e), and σ^2 is the log irradiance variance which depends on the channel's characteristics [14, 19]. Moreover, $\mathbb{1}_{\mathcal{D}}$ is the indicator function which signifies that the PDF is zero outside the domain \mathcal{D} . We note that in the above expression the irradiance is normalised, so that $\mathbb{E}[I] = 1$ and, consequently, $\bar{\gamma} = \eta^2/N_0$.

3.2 Gamma-gamma distribution

The PDF for the gamma-gamma irradiance is given by [4, 10]

$$f(I) = \frac{2(\alpha\beta)^{(\alpha+\beta)/2}}{\Gamma(\alpha)\Gamma(\beta)} I^{\alpha+\beta/2-1} K_{\alpha-\beta}(2\sqrt{\alpha\beta I}) \mathbb{1}_{(0,\infty)}, \quad (4)$$

where $\Gamma(z)$ is the gamma function and $K_\nu(z)$ is the modified Bessel function of the second kind [30]. In this case also, the average irradiance is $\mathbb{E}[I] = 1$. The two parameters α and β are decided by the atmospheric conditions [12, 20]. In case the optical radiation is assumed to be a plane wave, these parameters are given by [12, 20]

$$\alpha = \left[\exp\left(\frac{0.49\sigma_l^2}{(1 + 1.11\sigma_l^{12/5})^{7/6}}\right) - 1 \right]^{-1}, \quad (5)$$

$$\beta = \left[\exp\left(\frac{0.51\sigma_l^2}{(1 + 0.69\sigma_l^{12/5})^{5/6}}\right) - 1 \right]^{-1}. \quad (6)$$

Here $\sigma_l^2 = 1.23C_n^2 k^{7/6} L^{11/6}$ is the log irradiance variance, L is the link range, $k = 2\pi/\lambda$ is the wave number with λ being the wavelength, and C_n is the refractive index structure parameter which, for a horizontal link, is assigned a value $C_n^2 = 5 \times 10^{-13} \text{m}^{-2/3}$. Due to the presence of two parameters, gamma-gamma distribution has been found flexible enough to describe a wide range of turbulence conditions rather well, ranging from weak to strong [4, 10]. When either of the parameters α or β is unity, (4) reduces to the K distribution, which is discussed below.

3.3 K distribution

The K distribution has the PDF given by

$$f(I) = \frac{2\alpha^{(\alpha+1)/2}}{\Gamma(\alpha)} I^{(\alpha-1)/2} K_{\alpha-1}(2\sqrt{\alpha I}) \mathbb{1}_{(0,\infty)} \quad (7)$$

and, as can be seen, is a special case of the gamma-gamma distribution obtained for $\beta = 1$ in (4). In the limit $\alpha \rightarrow \infty$, it becomes a negative-exponential (e^{-I}) distribution. The K distribution is used to model strong turbulence conditions [5, 7, 10]. The corresponding theoretical predictions have been found to exhibit an excellent agreement with the experimental data [9].

4 Bit error rate

Noise, interference, distortion or bit synchronisation errors lead to undesirable alteration in the received bits of a data stream over a communication channel. BER is a QoS measure that indicates the number of bit errors per unit time.

There are several modulation schemes which are employed to transmit the optical signal in the FSOC [3, 20, 31–33]. The ON–OFF keying (OOK), in both the non-return to zero (NRZ) and return to zero (RZ) encodings, is one of the conventional techniques [33]. Another very important modulation scheme is L -pulse position modulation (L -PPM), where M binary bits are transmitted as a single light pulse in one out of $L = 2^M$ possible time slots with remaining slots being empty [32]. BPSK and QPSK are two of the most popular methods in phase shift keying (PSK) [3, 20, 33]. Pulse amplitude modulation (PAM) is yet another prominent modulation technique where information bits are encoded in the amplitude of the signal [3, 20].

The signal dependent BER in the above mentioned modulation schemes can be expressed in a unifying manner as [27]

$$\begin{aligned} \mathcal{B}(I) &= \frac{1}{a} \operatorname{erfc}\left(\frac{\gamma^{1/2}}{b}\right) \\ &= \frac{1}{a} \operatorname{erfc}\left(\frac{\eta I}{b\sqrt{N_0}}\right) = \frac{1}{a} \operatorname{erfc}\left(\frac{\bar{\gamma}^{1/2} I}{b}\right), \end{aligned} \quad (8)$$

where $\operatorname{erfc}(\cdot)$ is the complementary error function [30], and the values of parameters a and b are compiled in Table 1.

The PDF of the BER can be calculated as

$$\begin{aligned} p_B(B) &= \int_0^\infty \delta(B - \mathcal{B}(I)) f(I) dI \\ &= \frac{\pi^{1/2} ab}{2\bar{\gamma}^{1/2} \exp[-(\operatorname{erfc}^{-1}(aB))^2]} \\ &\quad \times \int_0^\infty \delta\left(I - \frac{b}{\bar{\gamma}^{1/2}} \operatorname{erfc}^{-1}(aB)\right) f(I) dI. \end{aligned} \quad (9)$$

In deriving the above result, we used (8) for $\mathcal{B}(I)$ and the following property of the Dirac delta function [30]:

$$\delta(\phi(x)) \equiv \sum_i \frac{\delta(x - x_i)}{|\phi'(x_i)|}. \quad (10)$$

Here x_i are the simple roots of the equation $\phi(x) = 0$. In this case, $B - \mathcal{B}(I) = 0$ yields the root as $I = (b/\bar{\gamma}^{1/2}) \operatorname{erfc}^{-1}(aB)$. The delta-function integral can now be performed easily to yield

$$\begin{aligned} p_B(B) &= \frac{\pi^{1/2} ab}{2\bar{\gamma}^{1/2}} \exp[(\operatorname{erfc}^{-1}(aB))^2] \\ &\quad \times f\left(\frac{b}{\bar{\gamma}^{1/2}} \operatorname{erfc}^{-1}(aB)\right) \mathbb{1}_{(0,1/a)}. \end{aligned} \quad (11)$$

Using the above general expression, we can deal with any fading model with the corresponding PDF of the irradiance given by $f(I)$. For instance, for the log-normal, gamma-gamma, and K distributions, we have the following explicit results, respectively,

$$p_B^{(LN)}(B) = \frac{a}{2\sqrt{2}\sigma \operatorname{erfc}^{-1}(aB)} \exp[(\operatorname{erfc}^{-1}(aB))^2] \times \exp\left[-\frac{1}{2\sigma^2} \left(\ln\left\{\frac{b}{\bar{\gamma}} \operatorname{erfc}^{-1}(aB)\right\} + \frac{\sigma^2}{2}\right)^2\right] \mathbb{1}_{(0, 1/a)} \quad (12)$$

$$p_B^{(GG)}(B) = \frac{\pi^{1/2} a (b\alpha\beta)^{(\alpha+\beta)/2}}{\bar{\gamma}^{\alpha+\beta/4} \Gamma(\alpha)\Gamma(\beta)} \times \exp[(\operatorname{erfc}^{-1}(aB))^2] (\operatorname{erfc}^{-1}(aB))^{\alpha+\beta/2-1} \times K_{\alpha-\beta} \left[2 \left(\frac{b\alpha\beta}{\bar{\gamma}^{1/2}} \operatorname{erfc}^{-1}(aB)\right)^{1/2}\right] \mathbb{1}_{(0, 1/a)} \quad (13)$$

$$p_B^{(K)}(B) = \frac{\pi^{1/2} a (b\alpha)^{(\alpha+1)/2}}{\bar{\gamma}^{\alpha+1/4} \Gamma(\alpha)} \times \exp[(\operatorname{erfc}^{-1}(aB))^2] (\operatorname{erfc}^{-1}(aB))^{\alpha-1/2} \times K_{\alpha-1} \left[2 \left(\frac{b\alpha}{\bar{\gamma}^{1/2}} \operatorname{erfc}^{-1}(aB)\right)^{1/2}\right] \mathbb{1}_{(0, 1/a)} \quad (14)$$

We will demonstrate below that there are circumstances when the actual probability of the BER value being close to the average value $\mathbb{E}[B] = \int_0^{1/a} B p_B(B) dB$ can be quite small. To quantify this, we consider the probability of BER being within the interval $[\mathbb{E}[B] - \delta_B, \mathbb{E}[B] + \delta_B]$ around the average $\mathbb{E}[B]$. This can be obtained using the integral

$$\Pi_B = \int_{\mathbb{E}[B] - \delta_B}^{\mathbb{E}[B] + \delta_B} p_B(B) dB \quad (15)$$

We would like to remark that, to study the dispersion of the probability distribution, one may be interested in calculating the coefficient of variation (CV), which is defined as the ratio of the standard deviation to the mean [34]. However, in the present investigation, the mean can get very close to zero (see, e.g. Table 2) and therefore CV may not serve as a good measure to capture the dispersion behaviour.

As indicated above, in the following, we focus on the BER using the BPSK ($a=2, b=1$) and QPSK ($a=1, b=1$) modulation schemes for log-normal, gamma-gamma, and K distributions. Other modulation schemes can be treated similarly. It may be noted from the general structure of the BER distribution appearing in (11) that the PDFs for the BPSK and QPSK modulation schemes are related to each other by a scaling of 2, since the variable B scales by the parameter a .

4.1 Results for log-normal irradiance

We use (12) with $\sigma = 0.3$ to analyse the BER PDF in the BPSK and QPSK modulation schemes. We show the corresponding PDF plots in Fig. 1 for two average SNR ($\bar{\gamma}$) values measured in dB. Monte Carlo simulation based results (overlaid symbols: filled circles and squares) are also displayed and are in conformity with the analytical results (solid curves). The Monte Carlo simulation involves generating 100,000 BER values using random numbers from the log-normal distribution and (8). The average BER value ($\mathbb{E}[B]$), rounded to three decimal places) corresponding to each curve is also indicated on the horizontal axis using an arrow. As discussed above, the scaling of two can be observed between the BPSK and QPSK curves, i.e. the QPSK curve extends up to twice the width of BPSK curve and has half the corresponding height.

In Table 2 we compile, for the BPSK modulation scheme, values of the average BER $\mathbb{E}[B]$, the variance $\operatorname{Var}[B] = \mathbb{E}(B^2) - (\mathbb{E}(B))^2$, and the probability Π_B of the BER being within a neighbourhood $\pm \delta_B$ of $\mathbb{E}[B]$. We choose $\delta_B = 0.05$, which corresponds to an interval of length 0.05 on either side of $\mathbb{E}[B]$, unless $\mathbb{E}[B]$ lies closer to the edges (0 or $1/a = 0.5$) than a distance of 0.05. It should be noted that 0.05 constitutes 10% of the total available domain of 0 to 0.5 for the BER in the BPSK scheme. We can see from the tabulation that in the log-normal model the

Table 2 BER statistics for BPSK modulation scheme in the log-normal irradiance model: $\mathbb{E}[B]$, $\operatorname{Var}[B]$, and Π_B for $\delta_B = 0.05$. For QPSK modulation scheme, the $\mathbb{E}[B]$ is twice and $\operatorname{Var}[B]$ is four times the values shown below for BPSK modulation. Moreover, the Π_B values indicated below hold for QPSK modulation if δ_B is chosen as 0.1

σ	$\bar{\gamma}$	$\mathbb{E}[B]$	$\operatorname{Var}[B]$	Π_B
0.1	0	0.08070	0.00042	0.98573
0.1	5	0.00730	0.00002	1.00000
0.1	10	0.00002	0.00000	1.00000
0.2	0	0.08663	0.00164	0.78029
0.2	5	0.01139	0.00017	0.99040
0.2	10	0.00017	0.00000	1.00000
0.3	0	0.09579	0.00350	0.56593
0.3	5	0.01825	0.00063	0.94488
0.3	10	0.00090	0.00001	0.99932

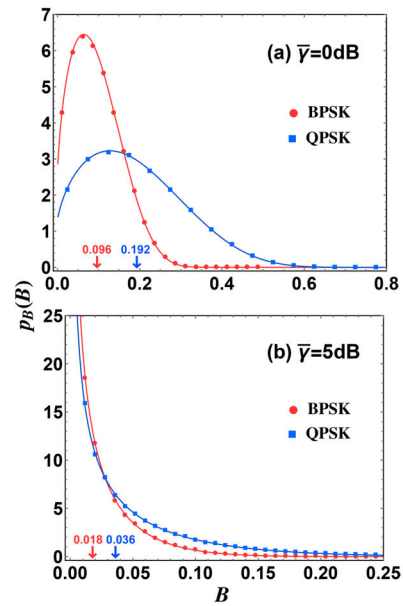


Fig. 1 PDF of the BER for the log-normal distributed irradiance in BPSK ($a=2, b=1$) and QPSK ($a=1, b=1$) modulation schemes. The log irradiance variance has been chosen as $\sigma = 0.3$. The solid curves indicate the analytical prediction and the overlaid symbols are based on Monte Carlo simulation. The average values of BER, indicated using the arrows pointing on the horizontal axes, are (a) BPSK: 0.096, QPSK: 0.192, (b) BPSK: 0.018, QPSK: 0.036

probability of the BER being within this interval, around the average value, is generally quite large. Hence, $\mathbb{E}[B]$ provides a reasonable estimate of the actual behaviour of the BER.

Due to the scaling relation between BPSK and QPSK schemes via the parameter a , the average and variance values for the latter are twice and four times the ones indicated in the Table 2, respectively. Moreover, the Π_B values given in the table work for QPSK if δ_B is chosen as 0.1 around the corresponding average value.

4.2 Results for gamma-gamma irradiance

We use (13) to analyse the BER distribution under the gamma-gamma irradiance model under the BPSK and QPSK modulation schemes. In Fig. 2, we show the BER PDFs for two average SNR ($\bar{\gamma}$) values in the gamma-gamma distribution with $\alpha = 4$ and $\beta = 2$. The curves based on analytical results match very well with the Monte Carlo simulation results depicted using symbols. The latter involves obtaining 100,000 BER values calculated using (8) with the aid of random numbers from the gamma-gamma distribution. In this case, we observe that the PDFs are quite dispersed about the average values indicated by the arrows pointing on the horizontal

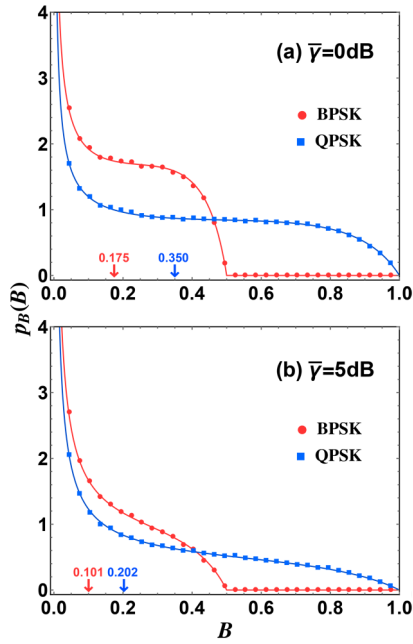


Fig. 2 PDF of the BER for the gamma-gamma distributed irradiance with $\alpha = 4, \beta = 2$ in the BPSK ($a = 2, b = 1$) and QPSK ($a = 1, b = 1$) modulation schemes. Solid curves are based on analytical expression, while the overlaid symbols are using Monte Carlo simulation. The average values of BER for the two plots, indicated using arrows, are (a) BPSK: 0.175, QPSK: 0.350, (b) BPSK: 0.101, QPSK: 0.202

Table 3 BER statistics for BPSK modulation scheme in the gamma-gamma irradiance model: $\mathbb{E}[B]$, $\text{Var}[B]$, and Π_B for $\delta_B = 0.05$. For QPSK modulation scheme, the $\mathbb{E}[B]$ is twice and $\text{Var}[B]$ is four times the values compiled below. The Π_B values appearing below hold for QPSK modulation if δ_B is taken as 0.1.

α	β	$\bar{\gamma}$	$\mathbb{E}[B]$	$\text{Var}[B]$	Π_B
2	2	0	0.19634	0.02547	0.15201
2	2	5	0.12521	0.02157	0.14138
2	2	10	0.07177	0.01452	0.15486
3	2	0	0.18272	0.02298	0.16589
3	2	5	0.10933	0.01824	0.16043
3	2	10	0.05740	0.01108	0.20995
3	3	0	0.16790	0.01986	0.18634
3	3	5	0.09199	0.01431	0.19291
3	3	10	0.04233	0.00739	0.83857
4	2	0	0.17524	0.02163	0.17451
4	2	5	0.10096	0.01654	0.17294
4	2	10	0.05041	0.00949	0.33436
4	3	0	0.15968	0.01814	0.19999
4	3	5	0.08278	0.01232	0.21747
4	3	10	0.03507	0.00575	0.85732
4	4	0	0.15100	0.01620	0.21775
4	4	5	0.07306	0.01017	0.25503
4	4	10	0.02773	0.00413	0.87828

axes. This implies that the average value may not give a good estimate about the behaviour of the BER. Additionally, the PDF of BER in this case exhibits some interesting features. For small average SNR, i.e. $\bar{\gamma} \rightarrow -\infty$ dB, it assumes large values near the right edge ($B = 1/2$ for BPSK and $B = 1$ for QPSK) and for large $\bar{\gamma}$ it shows enhanced values towards the left edge ($B = 0$). Correspondingly, the minimum of the PDF (anti-mode) in each case is located towards the left edge for small $\bar{\gamma}$ values and moves towards the right edge, as $\bar{\gamma}$ is increased to large values.

In Table 3, we tabulate Π_B for $\delta_B = 0.05$, along with $\mathbb{E}[B]$ and $\text{Var}[B]$, for several parameter values in the BPSK case. Here we

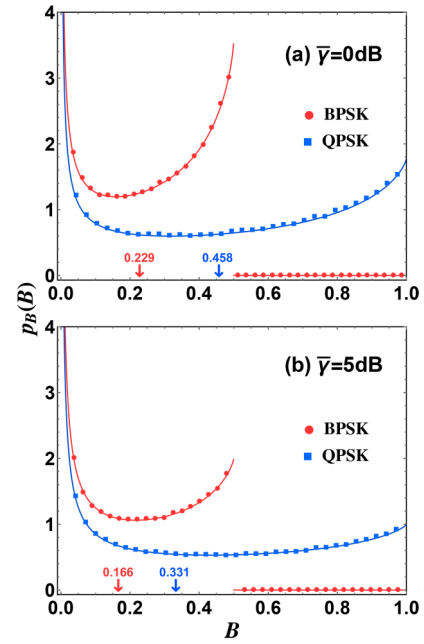


Fig. 3 PDF of the BER for the K -distributed irradiance with $\alpha = 2$ in the BPSK ($a = 2, b = 1$) and QPSK ($a = 1, b = 1$) modulation schemes. Solid curves are based on analytical expression and the overlaid symbols are using Monte Carlo simulation. The average values of BER for the two plots, indicated using arrows, are (a) BPSK: 0.229, QPSK: 0.458, (b) BPSK: 0.166, QPSK: 0.331

find that the probability of the BER assuming a value within a neighbourhood ± 0.05 of the average is typically low. This indicates that in this case the average BER is not a good indicator of the actual behaviour of the random variable B . It can be also seen that the variances in this case are comparatively larger. The results for QPSK case again follow using the scaling of 2.

4.3 Results for K -distributed irradiance

We investigate the BER statistics for K -distributed irradiance using (14). Fig. 3 depicts the plots for the BER PDF for BPSK and QPSK modulation schemes for two SNR values with the parameter α set to 2. The agreement between the solid curves using the analytical results and the symbols based on Monte Carlo simulation is excellent. Here also we see that the BER values are rather dispersed about the average values indicated using the arrows on the horizontal axes.

Table 4 compiles the $\mathbb{E}[B]$ and $\text{Var}[B]$ values along with Π_B for $\delta_B = 0.05$ valid for the BPSK modulation. Low Π_B values indicate that $\mathbb{E}[B]$ does not serve as a good measure for assessing the BER behaviour. A similar conclusion holds for the QPSK modulation scheme also due to the scaling relationship via the parameter a .

5 Channel capacity

Channel capacity is an important performance metric that refers to the maximum achievable data rate that can be reliably communicated between the transmitter and the receiver. It is given by [14, 15]

$$\mathcal{C}(I) = \frac{W}{\ln 2} \ln(1 + \gamma) = \frac{W}{\ln 2} \ln(1 + \bar{\gamma} I^2), \quad (16)$$

where W represents the bandwidth. The corresponding PDF can be calculated as

$$\begin{aligned}
p_C(C) &= \int_0^\infty \delta(C - \mathcal{E}(I))f(I) dI \\
&= \frac{2^{C/W-1} \ln 2}{W(2^{C/W} - 1)^{1/2} \bar{\gamma}^{1/2}} \\
&\quad \times \int_0^\infty \delta\left(I - \frac{(2^{C/W} - 1)^{1/2}}{\bar{\gamma}^{1/2}}\right) f(I) dI.
\end{aligned} \tag{17}$$

We used here (16) and the property of the Dirac delta function as in (10). This then readily yields

$$\begin{aligned}
p_C(C) &= \frac{2^{C/W-1} \ln 2}{W(2^{C/W} - 1)^{1/2} \bar{\gamma}^{1/2}} \\
&\quad \times f\left(\frac{(2^{C/W} - 1)^{1/2}}{\bar{\gamma}^{1/2}}\right) \mathbb{1}_{(0, \infty)}.
\end{aligned} \tag{18}$$

This equation can be used to evaluate the channel capacity PDF for any kind of turbulence scenario with the irradiance modelled by a function $f(I)$. In the cases of log-normal, gamma-gamma, and K distributions, it yields the following expressions, respectively,

$$\begin{aligned}
p_C^{(\text{LN})}(C) &= \frac{2^{C/W-1} \ln 2}{\sqrt{2\pi} \sigma W(2^{C/W} - 1)} \\
&\quad \times \exp\left[-\frac{1}{8\sigma^2} \left(\ln\left(\frac{2^{C/W} - 1}{\bar{\gamma}}\right) + \sigma\right)^2\right] \mathbb{1}_{(0, \infty)},
\end{aligned} \tag{19}$$

$$\begin{aligned}
p_C^{(\text{GG})}(C) &= \frac{2^{C/W} (\ln 2) (\alpha\beta)^{(\alpha+\beta)/2}}{W \bar{\gamma}^{\alpha+\beta/4} \Gamma(\alpha)\Gamma(\beta)} (2^{C/W} - 1)^{(\alpha+\beta)/4-1} \\
&\quad \times K_{\alpha-\beta} \left[2\sqrt{\alpha\beta} \left(\frac{2^{C/W} - 1}{\bar{\gamma}}\right)^{1/4} \right] \mathbb{1}_{(0, \infty)}.
\end{aligned} \tag{20}$$

$$\begin{aligned}
p_C^{(\text{K})}(C) &= \frac{2^{C/W} (\ln 2) \alpha^{\alpha+1/2}}{W \bar{\gamma}^{\alpha+1/4} \Gamma(\alpha)} (2^{C/W} - 1)^{(\alpha-3)/4} \\
&\quad \times K_{\alpha-1} \left[2\sqrt{\alpha} \left(\frac{2^{C/W} - 1}{\bar{\gamma}}\right)^{1/4} \right] \mathbb{1}_{(0, \infty)}.
\end{aligned} \tag{21}$$

It is convenient to define the channel capacity per bandwidth, $\tilde{C} = C/W$ [14, 15], for which the PDF is given by

$$\begin{aligned}
p_{\tilde{C}}(\tilde{C}) &= p_C(W\tilde{C}) \left| \frac{dC}{d\tilde{C}} \right| = W p_C(W\tilde{C}) \\
&= \frac{2^{\tilde{C}-1} \ln 2}{(2^{\tilde{C}} - 1)^{1/2} \bar{\gamma}^{1/2}} f\left(\frac{(2^{\tilde{C}} - 1)^{1/2}}{\bar{\gamma}^{1/2}}\right) \mathbb{1}_{(0, \infty)}.
\end{aligned} \tag{22}$$

We note that this expression is same as (18) with W effectively set to 1.

Similar to the BER analysis, we consider the probability of the channel capacity being within the interval $[\mathbb{E}[C] - \delta_C, \mathbb{E}[C] + \delta_C]$ in the neighbourhood of $\mathbb{E}[C]$. It is obtained using the integral

$$\Pi_C = \int_{\mathbb{E}[C] - \delta_C}^{\mathbb{E}[C] + \delta_C} p_C(C) dC. \tag{23}$$

Similar expression holds for the channel capacity per bandwidth (\tilde{C}). In the following three subsections, we analyse the behaviour of \tilde{C} for the log-normal, gamma-gamma, and K irradiance models.

5.1 Results for log-normal distributed irradiance

We show the plots of the channel capacity PDF in Fig. 4 for two average SNR ($\bar{\gamma}$) values for the log-normal distribution with log irradiance variance $\sigma = 0.3$. Monte Carlo simulation based symbols (filled diamonds) are overlaid on the analytical curves and are in excellent agreement. As in the case of the BER analysis, the Monte Carlo simulation involves generating 100,000 channel capacity

Table 4 BER statistics for BPSK modulation scheme in the K irradiance model: $\mathbb{E}[B]$, $\text{Var}[B]$, and Π_B for $\delta_B = 0.05$. For QPSK modulation scheme, the $\mathbb{E}[B]$ is twice and $\text{Var}[B]$ is four times the values compiled below for BPSK modulation. The Π_B values given below hold for QPSK modulation if δ_B is taken as 0.1

α	$\bar{\gamma}$	$\mathbb{E}[B]$	$\text{Var}[B]$	Π_B
1	0	0.25687	0.03409	0.11392
1	5	0.19927	0.03495	0.09680
1	10	0.14807	0.03169	0.08682
2	0	0.22914	0.03112	0.12637
2	5	0.16562	0.02992	0.10986
2	10	0.11282	0.02466	0.10257
3	0	0.21796	0.02988	0.13168
3	5	0.15279	0.02796	0.11541
3	10	0.10054	0.02220	0.10956

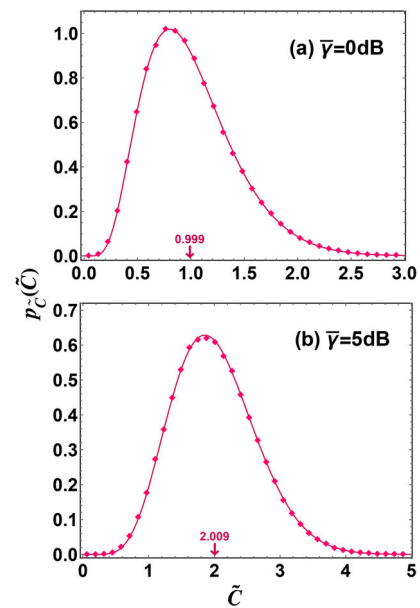


Fig. 4 PDF of the channel capacity per bandwidth for the log-normal distributed irradiance with $\sigma = 0.3$. The solid curves depict the analytical results and the overlaid symbols are based on Monte Carlo simulation. The average values $\mathbb{E}[\tilde{C}]$ for the two plots (a) 0.999, (b) 2.009, are indicated using arrows

values using random numbers taken from the log-normal distribution. The average channel capacity value ($\mathbb{E}[\tilde{C}] = \int_0^\infty \tilde{C} p_{\tilde{C}}(\tilde{C}) d\tilde{C}$) for each plot is also indicated on the horizontal axis using an arrow. From the plots, we can see that the channel capacity values are rather localised around $\mathbb{E}[\tilde{C}]$, considering the available domain $(0, \infty)$ for the channel capacity.

In Table 5, we consider the channel capacity per bandwidth and compile the corresponding average $\mathbb{E}[\tilde{C}]$, the variance $\text{Var}[\tilde{C}]$, and the probability $\Pi_{\tilde{C}}$ of the channel capacity being occurring within an interval $\delta_{\tilde{C}} = 0.5$ around $\mathbb{E}[\tilde{C}]$. Rather high values of $\Pi_{\tilde{C}}$ imply that $\mathbb{E}[\tilde{C}]$ is a good indicator of the channel capacity behaviour in the log-normal irradiance model for the considered parameter values.

5.2 Results for gamma-gamma distributed irradiance

We show the plots of channel capacity PDF in Fig. 5 considering the gamma-gamma fading model with $\alpha = 4$ and $\beta = 2$. The Monte Carlo results are also displayed using the symbols. In contrast to the log-normal case, here the distribution is rather spread out around the average values indicated using the arrows on the horizontal axes. Low $\Pi_{\tilde{C}}$ values in Table 6 and large variances also

Table 5 Channel capacity statistics in the log-normal irradiance model: $\mathbb{E}[\tilde{C}]$, $\text{Var}[\tilde{C}]$, and $\Pi_{\tilde{C}}$ for $\delta_{\tilde{C}} = 0.5$

σ	$\bar{\gamma}$	$\mathbb{E}[\tilde{C}]$	$\text{Var}[\tilde{C}]$	$\Pi_{\tilde{C}}$
0.1	0	0.99998	0.02071	0.99891
0.1	5	2.05171	0.04764	0.97830
0.1	10	3.44874	0.06849	0.94408
0.2	0	0.99973	0.08162	0.92843
0.2	5	2.03514	0.18585	0.75335
0.2	10	3.41711	0.27008	0.66211
0.3	0	0.99872	0.17927	0.78289
0.3	5	2.00869	0.40179	0.56288
0.3	10	3.36585	0.59308	0.47864

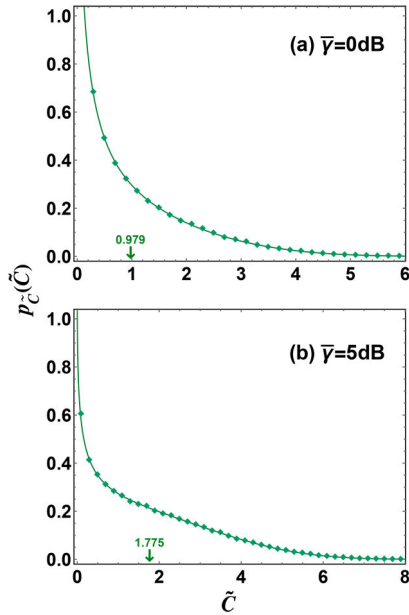


Fig. 5 PDF of the channel capacity per bandwidth for the gamma-gamma distributed irradiance with $\alpha = 4, \beta = 2$. Analytical predictions are illustrated using the solid curves and Monte Carlo simulation results are shown using the overlaid symbols. The average channel capacity values depicted using the arrows are (a) 0.979, (b) 1.775 for the two plots, respectively

Table 6 Channel capacity statistics in the gamma-gamma irradiance model: $\mathbb{E}[\tilde{C}]$, $\text{Var}[\tilde{C}]$, and $\Pi_{\tilde{C}}$ for $\delta_{\tilde{C}} = 0.5$

α	β	$\bar{\gamma}$	$\mathbb{E}[\tilde{C}]$	$\text{Var}[\tilde{C}]$	$\Pi_{\tilde{C}}$
2	2	0	0.96321	1.32108	0.27306
2	2	5	1.70444	2.67181	0.18492
2	2	10	2.71160	4.42655	0.15006
3	2	0	0.97317	1.16232	0.30026
3	2	5	1.74938	2.39271	0.20226
3	2	10	2.80576	3.95638	0.16438
3	3	0	0.98076	0.99164	0.33626
3	3	5	1.79495	2.07646	0.22534
3	3	10	2.90548	3.40880	0.18371
4	2	0	0.97870	1.07287	0.31707
4	2	5	1.77467	2.23403	0.21295
4	2	10	2.85784	3.69215	0.17315
4	3	0	0.98489	0.89542	0.35954
4	3	5	1.82075	1.89547	0.24033
4	3	10	2.96099	3.09876	0.19625
4	4	0	0.98818	0.79537	0.38782
4	4	5	1.84692	1.70090	0.25871
4	4	10	3.01862	2.76135	0.21176

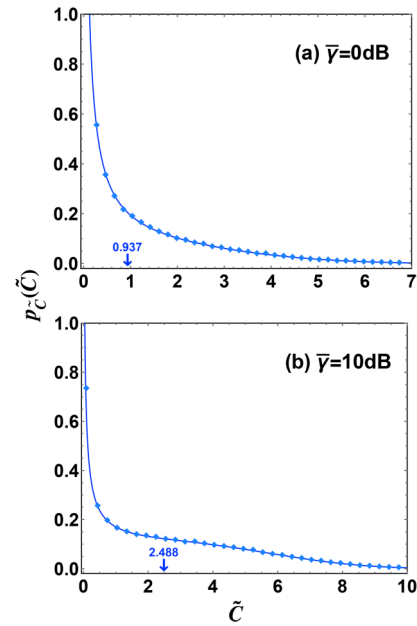


Fig. 6 PDF of the channel capacity per bandwidth for the K-distributed irradiance with $\alpha = 2$. Analytical predictions are illustrated using the solid curves and Monte Carlo simulation results are shown using the overlaid symbols. The average channel capacity values depicted using the arrows are (a) 0.937, (b) 2.488 for the two plots, respectively

Table 7 Channel capacity statistics in the K-distributed irradiance model: $\mathbb{E}[\tilde{C}]$, $\text{Var}[\tilde{C}]$, and $\Pi_{\tilde{C}}$ for $\delta_{\tilde{C}} = 0.5$

α	$\bar{\gamma}$	$\mathbb{E}[\tilde{C}]$	$\text{Var}[\tilde{C}]$	$\Pi_{\tilde{C}}$
1	0	0.90145	1.98533	0.18928
1	5	1.49409	3.74489	0.13076
1	10	2.28638	6.17143	0.10545
2	0	0.93735	1.68641	0.22099
2	5	1.59862	3.29136	0.15139
2	10	2.48804	5.46766	0.12220
3	0	0.95207	1.55604	0.23553
3	5	1.64254	3.08968	0.16059
3	10	2.57129	5.15623	0.12949

lead to the conclusion that in this case $\mathbb{E}[\tilde{C}]$ performs extremely poor at assessing the behaviour of the channel capacity. Consequently, one must examine the higher-order moments or the PDF itself.

5.3 Results for K-distributed irradiance

Finally, we examine the behaviour of the channel capacity in Fig. 6 for the K distribution with $\alpha = 2$. The analytical results shown using the solid curves are in excellent agreement with the overlaid symbols obtained using Monte Carlo simulation. As can be observed, the PDF curves are rather dispersed about the average values indicated using the arrows on the horizontal axes. The $\mathbb{E}[\tilde{C}]$ and $\text{Var}[\tilde{C}]$ values are compiled in Table 7 along with the $\Pi_{\tilde{C}}$ for $\delta_{\tilde{C}} = 0.5$. Low values for the $\Pi_{\tilde{C}}$ conform with the observation in the figure and thereby emphasise to look beyond the average for capturing the true behaviour of the channel capacity.

6 Conclusion

In this work, we have derived, for the first time, exact closed-form results for the PDFs of BER and channel capacity, which can be used for an arbitrary irradiance fading model. In particular, we have focused on the log-normal, gamma-gamma, and K distribution models and validated our analytical results using Monte Carlo simulations. In our analysis, we find that the averages of BER and channel capacity assess the overall behaviour of these

measures rather well for the log-normal model which applies to low turbulence conditions. However, for the case of gamma-gamma and K distributions with parameters set to model medium to strong turbulence conditions, the average values perform very poorly in capturing the actual behaviour of the BER and the channel capacity which are rather dispersed significantly around the mean. Consequently, we have argued that one must go beyond the lower moments and, in fact, investigate the full distribution to get a complete picture.

7 References

- [1] Khalighi, M.A., Uysal, M.: 'Survey on free space optical communication: a communication theory perspective', *IEEE Commun. Surv. Tutor.*, 2014, **16**, (4), pp. 2231–2258
- [2] Son, I.K., Mao, S.: 'A survey of free space optical networks', *Digital Commun. Netw. Sci. Direct*, 2016, **3**, pp. 67–77
- [3] Ghassemlooy, Z., Popoola, W., Rajbhandari, S.: 'Optical wireless communications: system and channel modelling with MATLAB' (CRC Press, New York, 1st edn., 2012)
- [4] Andrews, L.C., Phillips, R.L.: 'Laser beam propagation through random media?', vol. 52 (SPIE Press, Bellingham, WA, 2005)
- [5] Phillips, R.L., Andrews, L.C.: 'Measured statistics of laser-light scattering in atmospheric turbulence', *J. Opt. Soc. Am.*, 1981, **71**, (12), pp. 1440–1445
- [6] Zhu, X., Kahn, J.M.: 'Free-space optical communication through atmospheric turbulence channels', *IEEE Trans. Commun.*, 2002, **50**, (8), pp. 1293–1300
- [7] Jakeman, E., Pusey, P.N.: 'Significance of K distributions in scattering experiments', *Phys. Rev. Lett.*, 1978, **40**, (9), pp. 546–550
- [8] Parry, G., Pusey, P.N.: 'K distribution in atmospheric propagation of laser light', *J. Opt. Soc. Am.*, 1979, **69**, (5), pp. 796–798
- [9] Jakeman, E., Pusey, P.: 'A model for non-Rayleigh sea echo', *IEEE Trans. Antennas Propag.*, 1976, **24**, (6), pp. 806–814
- [10] Al-Habash, A., Andrews, L.C., Philips, R.L.: 'Mathematical model for the irradiance probability density function of a laser beam propagating through turbulent media', *Opt. Eng.*, 2001, **40**, (8), pp. 1554–1562
- [11] Majumdar, A.K.: 'Free-space laser communication performance in the atmospheric channel', *J. Opt. Fiber Commun. Rep.*, 2005, **2**, (4), pp. 345–396
- [12] Ghassemlooy, Z., Popoola, W.O., Leitgeb, E.: 'Free-space optical communication using subcarrier modulation in gamma-gamma atmospheric turbulence'. Proc. 9th Int. Conf. on Transparent Optical Networks (ICTON), Rome, Italy, 2007, vol. 3, pp. 156–160
- [13] Li, J., Uysal, M.: 'Optical wireless communications: system model, capacity and coding'. Proc. IEEE 58th Vehicular Technology Conf., Orlando, Florida, USA, October 2003, pp. 168–172
- [14] Katsis, A., Nistazakis, H.E., Tombras, G.S.: 'Bayesian and frequentist estimation of the performance of free space optical channels under weak turbulence conditions', *J. Franklin Inst.*, 2009, **346**, (4), pp. 315–327
- [15] Sandalidis, H.G., Tsiftsis, T.A.: 'Outage probability and ergodic capacity of free-space optical links over strong turbulence', *Electron. Lett.*, 2008, **44**, (1), pp. 46–47
- [16] Sandalidis, H.G., Tsiftsis, T.A., Karagiannidis, G.K., et al.: 'BER performance of FSO links over strong atmospheric turbulence channels with pointing errors', *IEEE Commun. Lett.*, 2008, **12**, (1), pp. 44–46
- [17] Kiasaleh, K.: 'Performance of coherent DPSK free-space optical communication systems in K-distributed turbulence', *IEEE Trans. Commun.*, 2006, **54**, (4), pp. 604–607
- [18] Navidpour, S.M., Uysal, M., Kavehrad, M.: 'BER performance of free-space optical transmission with spatial diversity', *IEEE Trans. Wireless Commun.*, 2007, **6**, (8), pp. 2813–2819
- [19] Nistazakis, H.E., Karagianni, E.A., Tsigopoulos, A.D., et al.: 'Average capacity of optical wireless communication systems over atmospheric turbulence channels', *J. Lightwave Technol.*, 2009, **27**, (8), pp. 974–979
- [20] Popoola, W.O., Ghassemlooy, Z.: 'BPSK subcarrier intensity modulated free-space optical communications in atmospheric turbulence', *J. Lightwave Technol.*, 2009, **27**, (8), pp. 967–973
- [21] Liu, C., Yao, Y., Sun, Y., et al.: 'Analysis of average capacity for free-space optical links with pointing errors over gamma-gamma turbulence channels', *Chin. Opt. Lett.*, 2010, **8**, (6), pp. 537–540
- [22] Liu, C., Yao, Y., Sun, Y., et al.: 'Average capacity for heterodyne FSO communication systems over Gamma-Gamma turbulence channels with pointing errors', *Electron. Lett.*, 2010, **46**, (12), pp. 851–853
- [23] Yi, X., Liu, Z., Yue, P.: 'Average BER of free-space optical systems in turbulent atmosphere with exponentiated Weibull distribution', *Opt. Lett.*, 2012, **37**, (24), pp. 5142–5144
- [24] Ansari, I.S., Alouini, M.-S., Cheng, J.: 'Ergodic capacity analysis of free-space optical links with nonzero boresight pointing errors', *IEEE Trans. Wirel. Commun.*, 2015, **14**, (8), pp. 4248–4264
- [25] Zhao, J., Zhao, S., Zhao, W., et al.: 'Average capacity of airborne optical links over exponentiated Weibull atmospheric turbulence channels', *Opt. Quantum Electron.*, 2017, **49**, p. 104
- [26] Singh, R.K., Karmeshu, S., Kumar, S.: 'A novel approximation for K distribution: closed-form BER using DPSK modulation in free-space optical communication', *IEEE Photon. J.*, 2017, **9**, (5), Art. no. 7906817, pp. 1–14
- [27] Singh, R.K., Kumar, S., Karmeshu, S.: 'A new approximation for PDF of K distribution: analytical study of QoS parameters in free space optical communication', *IET Commun.*, 2018, **12**, (14), pp. 1703–1708
- [28] Laourine, A., Stéphanne, A., Affes, S.: 'On the capacity of log-normal fading channels', *IEEE Trans. Commun.*, 2009, **57**, (6), pp. 1603–1607
- [29] Karmeshu, S., Khandelwal, V.: 'On the applicability of average channel capacity in log-normal fading environment', *Wireless Pers. Commun.*, 2013, **68**, (4), pp. 1393–1402
- [30] Arfken, G.B., Weber, H.J., Harris, F.E.: 'Mathematical methods for physicists' (Elsevier, New York, 2013, 7th edn.)
- [31] Wang, Z., Zhong, W.D., Fu, S., et al.: 'Performance comparison of different modulation formats over free-space optical (FSO) turbulence links with space diversity reception technique', *IEEE Photonics J.*, 2009, **1**, (6), pp. 277–285
- [32] Audeh, M.D., Kahn, J.M.: 'Performance evaluation of L-pulse position modulation on nondirected indoor infrared channels'. Proc. Int. Conf. Communication, New Orleans, Louisiana, USA, May 1994, vol. 2, pp. 660–664
- [33] Majumdar, A.K.: 'Free-space optical (FSO) platforms: unmanned aerial vehicle (UAV) and mobile', in 'Advanced Free space optics (FSO)', Springer series in optical sciences (Springer-Verlag, New York, USA, 2015), pp. 203–225
- [34] Everitt, B.S.: 'The Cambridge dictionary of statistics' (Cambridge University Press, Cambridge, UK, 1995)